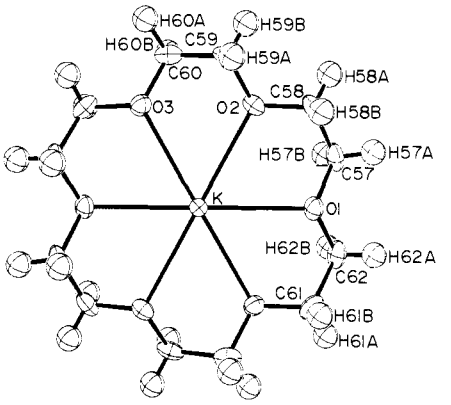

Figure 2. Structure and numbering system of the potassium 18-crown-6 cation.

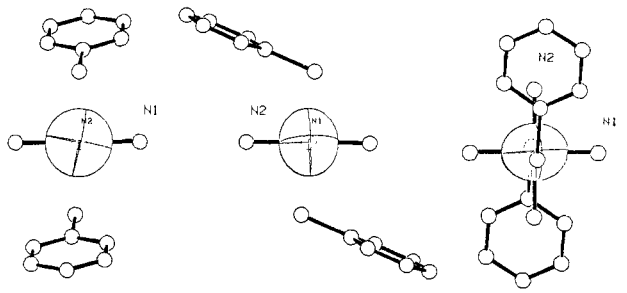

Figure 3. Ellipsoid representation of the **g** tensor viewed along three molecular axes.

ESR Measurements. In the right-handed coordinate system in which x corresponds to the N(2) to Fe direction and y corresponds to the Fe to N(1) direction, the experimentally determined elements of $\mathbf{g}^2$ are $\langle g^2\rangle_{11} = 3.865$, $\langle g^2\rangle_{22} = 4.918$, $\langle g^2\rangle_{33} = 5.432$, $\langle g_2\rangle_{12} = -0.074$, and $\langle g^2\rangle_{23} = 0.111$. Diagonalization of this tensor gives principle g values of 1.964, 2.213, and 2.337,[13] in reasonable agreement with values of 1.960, 2.216, and 2.335 obtained from a polycrystalline spectrum without correction for lineshape.

Figure 3 illustrates the orientation of the **g** tensor in the complex. As previously observed in the study of ferric heme proteins, the principle axis corresponding to the largest g is within 15° (in this case 12°) of the normal to the porphyrin plane. Perhaps more significant is the observation that the principle axis corresponding to the smallest g value is only 4° from the Fe–N(2) direction. Taylor[2] has demonstrated that, neglecting spin–orbit coupling and covalency,[14] the partially occupied d orbital in low-spin Fe(III) systems of this type lies in the plane defined by the two largest principle g values. This corresponds closely to the d_{yz} orbital in the molecular axis coordinate system defined above. The inference that the d_{yz} orbital is higher in energy than either d_{xz} or d_{xy} is easily rationalized as a consequence of its interaction with filled p orbitals on the ligand sulfur atoms. Since the α-carbon of the benzene thiolate is not far from the plane defined by Fe, N(2), and S, it is entirely reasonable that the axis corresponding to the smallest g value lies close to the Fe–N(2) direction. However, it must be pointed out that before any useful generalization can be constructed concerning the orientation of the **g** tensor in materials of this kind, it will be necessary to examine a material in which the axial ligand takes on a less symmetric orientation. It is conceivable that there is an indirect interaction between the iron ion and the thiolate ligand that involves the prophyrin ligand. If such an interaction is predominant, one would expect the **g** tensor to be aligned with the porphyrin rather than the thiolate ligand.

Because the displacements of the principle axes of the **g** tensor from the idealized molecular axes (Figure 3) are not large compared to the experimental uncertainties, it is difficult to ascribe these displacements to specific distortions of the complex. As more data on related complexes becomes available, however, it may be possible to relate these displacements to various types of structural asymmetry.

Acknowledgment. This work was supported by the UCLA Research Committee, the UCLA Office of Academic Computing, and the National Science Foundation (Grant CHE79-06343). We thank the donors of the Petroleum Research Fund, administered by the American Chemical Society, for partial support of this research. Charles E. Strouse acknowledges the support of an Alfred P. Sloan research fellowship.

Supplementary Material Available: Tables II–VI and a listing of observed and calculated structure factors (15 pages). Ordering information is given on any current masthead page.

(13) The ordering here is the "common" ordering with g_x smallest and g_z largest. See ref 12 or Bohan, T. L. *J. Magn. Reson.* **1977**, *26*, 109–118 for the "proper" choice of coordinate system and assignment of signs.

(14) Analysis[2] of the principle g values provides squared coefficients in the ground-state wave functions of 1.001, 0.007, and 0.003 for the three real d orbitals defined in the principle axis coordinate system. Since these coefficients are nearly normalized and since contributions from the second two atomic orbitals are small, neither covalency nor spin–orbit induced mixing appear to be significant.

Linear to Bent Geometry Changes in Gas- and Solution-Phase Photochemistry of Tricarbonylnitrosylcobalt

Wayne Evans and Jeffrey I. Zink*

Contribution from the Department of Chemistry, University of California, Los Angeles, California 90024. *Received July 31, 1980*

Abstract: Photochemical reactions of $Co(CO)_3NO$ in both the gas and solution phases are reported and interpreted in terms of a bent cobalt–nitrosyl unit in the excited state. The molecular orbital reasons for expecting a bent excited state are discussed. In the gas phase, two types of photochemical reactions are observed: reactions at the coordinated nitrosyl and carbonyl exchange. The reaction with gaseous HCl produces the disproportionation products of HNO, N_2O, and H_2O. This reaction is interpreted in terms of an "NO^-" photointermediate. In both the gas and solution phases, associative carbonyl-exchange reactions with Lewis base entering ligands are observed. The solution-phase photoreactions are quantitatively treated by using kinetic theory and discussed in terms of a bent excited state.

The photochemistry of metal–nitrosyl complexes is of interest not only because of the potential for unusual photoreactions arising from excited-state geometry changes in the MNO group, the subject of this paper, but also because nitrosyl photochemistry

0002-7863/81/1503-2635$01.25/0

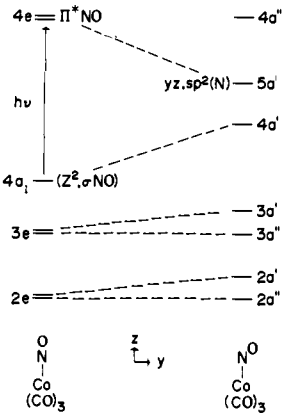

Figure 1. Correlation diagram for the linear (left) and bent (right) geometries of the CoNO unit in $Co(CO)_3NO$.

forms a part of the larger field of charge-transfer photochemistry. Qualitative and quantitative photochemical reactions of only a handful of metal–nitrosyl complexes have been reported. Three types of reactions have been observed. First, photoinduced expulsion of nitric oxide occurs from $Fe(das)_2(NO)X_2^{2+}$ [1] and $Fe(CN)_2(NO)^{2-}$ [2] in solution and NiCp (NO)[3] in inert gas matrices. Carbonyl photosubstitution or expulsion is observed from $Mn(CO)_4NO$[4] and $Co(CO)_3NO$[5-7] in solution and $Co(CO)_3NO$, $Mn(CO)_4(NO)$,[9] $MnCO(NO)_3$,[10] and $Fe(NO)_2(CO)_2$[11] in inert-gas matrices. Finally, reaction of the NO group was observed in $MoCpNO(CO)_2$[12] When viewed as an aspect of charge-transfer excited-state photochemistry, the nitrosyl complexes potentially offer a variety of systems containing low-lying metal to ligand charge-transfer excited states. In general, charge-transfer excited states are expected to lead to photoreactions which are interpretable in terms of oxidized or reduced metal centers and ligands.[13-16]

In a study of the photoreactions of $Fe(das)_2(NO)X^+$, we proposed that the populated MNO charge-transfer excited state could cause a geometry change in the MNO unit leading to the observed photoreactions.[1] An excited-state geometry change is expected to be a general feature of MNO units from the Enemark–Feltham interpretation of the MNO group.[17] Rest has suggested that certain IR bands observed in low-temperature matrices containing photolyzed metal–nitrosyl complexes could be interpreted in terms of trapped species containing deformed MNO bonds.[9,10] In this paper, we report the gas- and solution-phase photochemistry of $Co(CO)_3NO$. The molecular orbital reasoning suggesting a linear to bent geometry change in the charge-transfer excited state is discussed. Photoreactions, including both reactions of the nitrosyl ligand and carbonyl substitution, are discussed in terms of the geometry change in the excited state.

Theory

The description of the Co–NO bonding in $Co(CO)_3NO$ which will be adopted here is that developed by Enemark and Feltham.[17] According to this picture, the metal–nitrosyl unit is considered to be an inorganic structural unit designated $\{MNO\}^{10}$.[18] A simplified energy level diagram for the $\{MNO\}^{10}$ unit is shown in Figure 1. In the ground electronic state, the Co–NO bond in $Co(CO)_3NO$ is linear and the HOMO is the $4a_1$ orbital. The LUMO is the 4e orbital which is mainly NO π antibonding in character. This molecular orbital description avoids the problem of assigning oxidation states to the metal and nitrosyl. In a limiting valence bond description, the linear Co–NO unit would be described as containing a NO^+ ligand. In the remainder of this paper, the description of the NO ligand as either NO^+ or NO^- will be used for illustrative purposes with the realization that the molecular orbital description is more accurate.

In the lowest energy electronic excited state, the Co–NO geometry is expected to change. The electronic transition corresponds to a cobalt to nitrosyl charge transfer, $4a_1 \rightarrow 4e$, which is primarily metal d_{z^2} to nitrosyl π antibonding in character. According to the correlation diagram in Figure 1, the charge-transfer excitation should cause a linear to bent Co–NO geometry change. In addition, the tetrahedral coordination geometry is expected to become planar. The driving force for the linear to bent geometry change is the population of an orbital which is π antibonding between the metal and the NO in the linear geometry but π bonding and thus more stable in the bent geometry.

There are two photochemically significant properties which are induced by a linear to bent geometry change. First, the formally NO^+ ligand of the ground state becomes a formally NO^- ligand in the excited state. The photochemical consequence is that electrophillic attack on the nitrosyl ligand in the excited state can be expected. Second, the formally Co(1–) metal in the ground state becomes a formally Co(1+) metal in the excited state; i.e., in a formal sense the metal has undergone a two-electron oxidation. One consequence is that the metal could be subjected to nucleophillic attack in the excited state. When stated in the MO language, irradiating the charge-transfer band populates the 4e orbital which causes the Co–NO bond to bend which in turn causes the 2e orbital metal *yz* and *xz* in character to become mainly nitrosyl sp^2 and π_y^* in character. These changes shift a pair of electrons from an orbital mainly d_{z^2} in character to one mainly d_{xz} in character, leaving a vacated d_{z^2} orbital available for bonding. These electronic changes increase the positive charge on the cobalt and decrease it on the nitrosyl.

Geometry changes caused by populating MNO π antibonding orbitals using chemical, electrochemical, and photochemical techniques are known or have been proposed. The best established chemical example is addition of a halide ion to linear $Co(das)_2(NO)^{2+}$ to produce $Co(das)_2(NO)X^+$ containing a strongly bent MNO unit.[19,20] In this example the π antibonding orbital is populated by the pair of electrons from the halide ligand. An important electrochemical example is the one-electron oxidation of $Fe(das)_2(NO)X^+$ where the geometry changes from bent to linear upon removal of the electron.[17] The most relevent aspect is that the *one*-electron oxidation results in a formal *two*-electron increase in positive charge on the nitrosyl group and one-electron decrease in the formal charge on the iron atom. In an electrochemical study on $Co(CO)_3NO$, a one-electron reduction populates the π antibonding orbital which causes a geometry change to a bent MNO unit. The formally NO^- ligand abstracts a proton from protogenic solvents to yield an unstable coordinated nitroxyl which undergoes further reactions.[21] Examples of photochemical reactions where irradiation of the charge transfer band caused the π antibonding orbital to be populated were discussed above. In all of these examples, the effect of an added ligand, added (or removed) electrons, or electrons "moved" by electronic transitions causes changes in the population of the π antibonding orbital which in turn causes geometry changes. It is noteworthy that one-

(1) Liu, P. H.; Zink, J. I. *Inorg. Chem.* **1977**, *16*, 3165.
(2) Wolfe, S. K.; Swinehart *Inorg. Chem.* **1975**, *14*, 1049.
(3) Crichton, O.; Rest, A. J. *J. Chem. Soc., Dalton Trans.* **1977**, *986*.
(4) (a) Treichel, P. M.; Pitcher, E.; King, R. B.; Stone, F. G. A. *J. Am. Chem. Soc.* **1961**, *83*, 2593. (b) Keeton, D. P.; Basolo, F. *Inorg. Chim. Acta.* **1972**, *6*, 33.
(5) Strohmeier, W.; vonHobe, P. *Z. Naturforsch., A* **1963**, *18A*, 770.
(6) Clark, R. J. *Inorg. Chem.* **1967**, *6*, 299.
(7) Sabherwal, I. H.; Burg, A. *J. Chem. Soc. D* **1969**, 853.
(8) Crichton, O.; Rest, A. J. *J. Chem. Soc., Dalton Trans.* **1977**, 536.
(9) Crichton, O.; Rest, A. J. *J. Chem. Soc., Dalton Trans.* **1977**, 208.
(10) Crichton, O.; Rest, A. J. *J. Chem. Soc., Dalton Trans.* **1977**, 202.
(11) Crichton, O.; Rest, A. J. *J. Chem. Soc., Dalton Trans.* **1977**, 656.
(12) McPhail, A. T.; Knox, G. R.; Robertson, C. G.; Sim, G. A. *J. Chem. Soc. A* **1971**, 205.
(13) Schwendiman, D. P.; Zink, J. I. *J. Am. Chem. Soc.* **1976**, *98*, 4439.
(14) Liu, P. H.; Zink, J. I. *J. Am. Chem. Soc.* **1977**, *99*, 2155.
(15) Mann, K. R.; Gray, H. B.; Hammond, G. S. *J. Am. Chem. Soc.* **1977**, *99*, 306.
(16) Adamson, A. W.; Fleischauer, P. D. "Concepts of Inorganic Photochemistry"; Wiley: New York, 1975; Chapter 3.
(17) Enemark, J. H.; Feltham, R. D. *Coord. Chem. Rev.* **1974**, *13*, 339.
(18) This formalism designates the number of d electrons on the metal when the nitrosyl ligand is formally NO^+.[17]
(19) Enemark, J. H.; Feltham, R. D. *Proc. Natl. Acad. Sci. U.S.A.* **1972**, *69*, 3534.
(20) Feltham, R. D.; Nyholm, R. S. *Inorg. Chem.* **1965**, *4*, 1334.
(21) Fofanni, A. *Z. Phys. Chem. (Wiesbaden)* **1968**, *60*, 167.

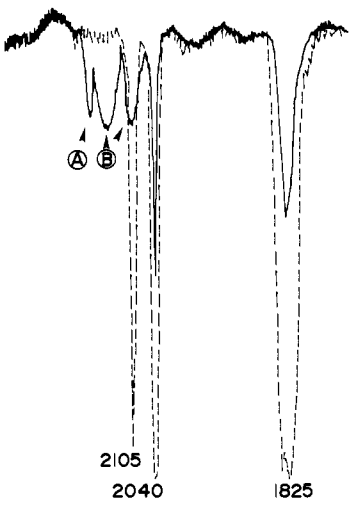

Figure 2. Infrared absorption spectra of unirradiated $Co(CO)_3NO$ (dotted lines) in the gas phase and gaseous $Co(CO)_3NO$ irradiated for 10 min in the presence of HCl (solid lines.) The peak labeled A is the P branch of the N_2O absorption and the peaks labeled B are the P and R branches of free CO. The R branch of N_2O and the P branch of CO overlap.

electron redox and one-electron electronic transitions cause formal two-electron changes on the metal and the nitrosyl ligand.

Results

(1) Gas-Phase Photochemistry. Three types of photoreactions are observed in the gas phase. First and most importantly, in the presence of hydrogen chloride the nitrosyl ligand reacts to produce nitrous oxide. Other reactions of the nitrosyl ligand are observed in the presence of oxygen, nitric oxide, and chloromethane. Second, carbonyl substitution is observed in the presence of the Lewis bases pyridine and triethylphosphine. Finally, in the presence of inert gases such as argon and nitrogen, the starting complex decomposes into cobalt metal and the consitituent ligands.

Nitrosyl Reactions. In the presence of HCl gas, the starting material reacts as shown in eq 1. Cobalt chloride is recovered

$$Co(CO)_3NO \xrightarrow[HCl\ gas]{h\nu} CoCl_2 + N_2O + H_2O + CO \quad (1)$$

as a solid photoproduct, nitrous oxide is observed in the gas phase by using infrared spectroscopy, and water is found by IR in the solid photoproduct. The gas-phase IR spectral changes accompanying the reaction are shown in Figure 2.

In the presence of oxygen, a second reaction of NO occurs to produce gaseous NO_2 and nitrate ion in the solid photoproduct. The solid product contains cobalt ions, probably as the oxide and as the nitrate salt. In the presence of chloromethane, a solid photoproduct containing $CoCl_2$ and a gaseous product with an IR band at 1260 cm^{-1} is produced. No nitrous oxide or nitric oxide is observed.

Carbonyl Photosubstitution. Carbonyl photosubstitution is the dominant photoreaction in the presence of pyridine and triethylphosphine as shown in eq 2. The efficiency of the photo-

$$Co(CO)_3NO \xrightarrow[L = PEt_3,\ py]{h\nu,\ gas} Co(CO)_2L(NO) \quad (2)$$

reaction is dependent on the ligand concentration as given in Table I. Under an atmosphere of carbon monoxide, no detectable photoreaction is observed. Carbon monoxide significantly depresses the reaction rate when mixed with the other gases which give rise to photochemical reactions.

Decomposition. In the presence of argon, nitrogen, or hydrogen, the starting material decomposes into the metal, carbon monoxide, and nitric oxide as shown in eq 3. A fine powder precipitates

$$Co(CO)_3NO \xrightarrow[Ar,\ N_2,\ or\ H_2]{h\nu} Co + NO + CO \quad (3)$$

to the bottom of the cell and a mirror forms on the entrance window. This decomposition is about 3 orders of magnitude less efficient than the other reactions discussed above as shown in Table I.

Table I. Relative Gas-Phase Photoreaction Quantum Yields

reagent gas	amount in cell	type of reaction[a]	relative ϕ[b]
O_4	1 atm	nitrosyl	1.00
PEt_3	8.0×10^{-6} mol[c]	sub	1.0
PEt_3	3.4×10^{-6} mol[c]	sub	0.67
PEt_3	2.5×10^{-6} mol[c]	sub	0.48
NO	1 atm	nitrosyl	0.39
pyr	3.4×10^{-6} mol[c]	sub	0.38
HCl	1 atm	nitrosyl	0.14
MeCl	1 atm	nitrosyl	0.12
H_2	1 atm	decomp	0.003
Ar	1 atm	decomp	0.001
N_2	1 atm	decomp	0.001
CO	1 atm	none	0.00001

[a] Nitrosyl = reaction of the nitrosyl ligand; i.e., the photoproduct is not NO. sub = carbonyl substitution. decomp = formation of Co, CO, and NO. [b] The $Co(CO)_3NO$ concentration is 4.0×10^{-6} M. [c] The supporting gas is H_2.

Table II. Solution-Phase Carbonyl Substitution Quantum Yields[a]

[L][b]	ϕ (L = PPh_3)	ϕ (L = $AsPh_3$)	ϕ (L = py)
0	0.0021	0.0021	0.0021
0.02	0.0370	0.0120	0.0165
0.04	0.0250	0.0250	0.0260
0.06	0.0585	0.0335	0.0300
0.08	0.0715	0.0455	0.0335
0.10	0.0860	0.0550	0.0355
0.12	0.125	0.0685	0.0405
0.15	0.130	0.0795	0.0390
0.20	0.170	0.105	0.0505
0.25	0.205	0.120	0.0690
0.30	0.240	0.145	0.0700
0.35	0.265	0.155	0.0810
0.40	0.275	0.160	0.0785
0.45	0.280	0.170	0.0845
0.50	0.295	0.180	0.0890

[a] All values are the average of at least two determinations and are accurate to ±10%. [b] Ligand to $Co(CO)_3NO$ concentration ratio. The metal concentration was 6.75×10^{-3} M in cyclohexane.

Table III. Infrared Stretching Frequencies

L in $CoNO(CO)_2L$	ν(CO), cm^{-1}	ν(NO), cm^{-1}	other bands
CO (soln)[a]	2110, 2042	1802	
PPh_3 (soln)[a]	2038, 1981	1750	
$AsPh_3$ (soln)[a]	2047, 1986	1756	
pyridine (soln)[a]	2041, 1969	1733	
CO (gas)	2105, 2040	1825	
PEt (gas)	2032, 1969	1747	
py (gas)	2041, 1969	1733	
pure gases			
NO			1876
N_2O			2222, 1275
NO_2			1610, 1250
NOCl			1800
CO			2150

[a] In cyclohexane.

Relative Quantum Yields. Gas-phase photoreaction quantum yields, relative to that of the reaction with oxygen, are given in Table I. Absolute quantum yields were not determined. For each reactant, a linear plot of degree of conversion vs. number of photons absorbed is found.

(2) Solution-Phase Photochemistry. $Co(CO)_3NO$ is highly photoactive when irradiated at 405 nm in the presence of Lewis base entering ligands L. When L is PPh_3, $AsPPh_3$, and pyridine, the ligand substitution reaction given in eq 4 is observed. The quantum yields for the reactions are strongly ligand dependent

$$Co(CO)_3NO \xrightarrow[L]{h\nu} Co(CO)_2LNO + CO \quad (4)$$

and ligand concentration dependent as shown in Table II.

The primary photosubstitution products, $Co(CO)_2L(NO)$, are monitored by following the appearance of the characteristic infrared absorption bands.[19,20] The decrease of the concentration of the starting material equals the increase in the concentration of the photoproduct within the limits of experimental error.

In the absence of an entering ligand, the starting material is much less photoactive with a quantum yield several orders of magnitude smaller than those of the typical photosubstitution reactions. This minor photoreaction pathway is independent of the concentration of the starting material.

Continued photolysis of $Co(CO)_3NO$ in the presence of L leads to production of $Co(CO)L_2NO$ and higher substitution products. In the studies reported here, interference from these secondary photolysis products was minimized by carrying out the photolysis to less than 20% conversion. When the reaction was carried out in chloroform and L = triphenylphosphine, continued photolysis led to the formation of CoL_2Cl_2.[21] All reactions reported here were carried out in cyclohexane.

(3) Spectra. The lowest energy electronic absorption features of $Co(CO)_3NO$ in cyclohexane consist of a weak band at 380 nm with a molar absorptivity of 7.5×10^2 M^{-1} cm^{-1} and a shoulder at about 460 nm. At least one shoulder occurs at higher energy at about 280 nm. For comparison, the isoelectronic cobalt-tetracarbonyl anion, $Co(CO)_4^-$ (as the PPN salt) has intense absorption bands ($\epsilon \gg 10^5$) at 206, 225, and 287 nm.[26] Luminescence of the pure liquid $Co(CO)_3NO$ could not be detected with standard instrumentation.

Discussion

Gas-Phase Photochemistry. The most important photochemical probe of the nature of the excited state of $Co(CO)_3NO$ is provided by its gas-phase reaction with HCl. The ground state contains a linear "NO^+-like" MNO unit. If the excited state consisted primarily of an activated NO^+ unit, the photoreaction with HCl would be expected to produce stable nitrosyl chloride, NO^+Cl^- as shown in eq 5. On the other hand, if the photoexcitation

$$Co\text{–}NO^+ \xrightarrow[Cl^-]{h\nu} NOCl \quad (5)$$

produces a bent MNO unit containing a NO^--like nitrosyl, the photoreaction with HCl would be expected to yield the unstable H^+NO^- molecule which disproportionates[27] into N_2O and H_2O as shown in eq 6.

$$Co^+\text{—}N(O)^- \xrightarrow[H^+]{h\nu} [HNO] \rightarrow {}^1/_2H_2O + {}^1/_2N_2O \quad (6)$$

When $Co(CO)_3NO$ is irradiated into its charge-transfer band in the presence of gaseous HCl, N_2O, cobalt(II) chloride, and water are efficiently produced. No appreciable thermal reactions are observed within the time span of the photochemical experiment. No NOCl is observed. A NO radical-like excited state would probably produce NOCl. When NO and HCl are mixed in the reaction cell, a slow thermal reaction produces NOCl but no photoreaction occurs at the wavelengths used for irradiation. The gas-phase photochemical reactions strongly support the formation of the photoactive excited state as a bent MNO unit containing a formally "NO^-"-like nitrosyl.

The observed photoreaction cannot distinguish between a bound "NO" ligand and a $Co(CO)_3{}^+NO^-$ ion pair. Although it would be surprising if the strong cobalt–nitrogen bond was ruptured by 405-nm light, the possibility is ruled out experimentally by the absence of any observed current when the reaction is carried out between electrically charged plates. An electric field up to 400 V/cm^{-1}, eight times larger than that typically used to detect ions in gaseous media, was used. Current detection limits were on the order of 100 pA. No current flow was detected.

The other gas-phase reactions listed in Table I are consistent with the bent CoNO excited state but cannot be interpreted as directly as can the reaction with HCl. The efficient photoreaction with CH_3Cl does not produce NOCl. Thus a linear NO^+ unit is not implicated. The efficient reaction with NO indirectly negates the intermediacy of a coordinated "NO" group because nitric oxide itself is not photoactive at these wavelengths. The ligand exchange photoreactions with triethylphosphine and with pyridine are consistent with associative attack on the formally Co(I) center in the excited state. The ligand-exchange reactions are quantitatively interpreted below.

Solution-Phase Photochemistry. In the solution phase, no reactions of the coordinated nitrosyl ligand are observed. Thus, the solution photochemistry does not provide as direct chemical evidence for the participation of a bent "NO^-" nitrosyl as does the gas-phase photochemistry. However, in a formal electron-counting sense, a bent MNO excited state produces a coordinatively unsaturated metal which, among other reactions, could undergo associative nucleophillic attack. The observed associative solution-phase carbonyl-exchange photoreaction can thus provide additional support for the bent MNO excited state.

The quantum yield of the ligand-exchange photoreaction in solution is strongly dependent on the type of entering ligand (e.g., phosphine, arsine, or pyridine) and on the concentration of the entering ligand. Three limiting mechanisms, associative (A),[28] associative interchange (IA),[28] and dissociative, are given in eq 7–9. The formal difference between the associative and associative

$$(A)\ Co(CO)_3NO \underset{k_1}{\overset{I_a\phi_o}{\rightleftharpoons}} [(CO)_3Co\text{—}NO] \xrightarrow{k_s[L]} [(CO)_3CoL(NO)] \xrightarrow{k_p} (CO)_2Co(NO)L \quad (7)$$

(k_b: $[(CO)_3Co\text{—}NO] \rightarrow Co(CO)_3NO$)

$$(IA)\ Co(CO)_3NO \underset{k_1}{\overset{I_a\phi_o}{\rightleftharpoons}} [(CO)_3Co\text{—}NO] \xrightarrow{k_2[L]} (CO)_2CoL(NO) \quad (8)$$

$$(D)\ Co(CO)_3NO \underset{k_1}{\overset{I_a\phi_o}{\rightleftharpoons}} [(CO)_2Co\text{—}NO + CO] \xrightarrow{k_3[L]} (CO)_2CoL(NO) \quad (9)$$

interchange mechanisms is the formation of a discrete five-coordinate intermediate in the former.[24]

In all of the above mechanisms, a reactive intermediate is formed with a quantum yield ϕ_o from the linear metal nitrosyl when I photons are absorbed. The reactive intermediate can undergo deactivation back to the ground state with a rate constant k_1. Competing with deactivation is a reaction with the entering ligand L (with a concentration [L]) to produce either a five-coordinate complex with rate constant k_5 in the associative mechanism or the photoproduct with a rate constant k_2 in the associative interchange mechanism. In the associative mechanism, the five-coordinate intermediate can either lose the ligand L with a composite rate constant k_b to regenerate the starting material or lose CO with a rate constant k_p to produce the observed photosubstitution product. In the dissociative mechanism, a carbon monoxide ligand is directly dissociated to produce a solvent caged pair. Reaction of the three-coordinate intermediate with ligand L competes with the recombination of the intermediate with CO. A solvent caged pair of some sort must be proposed for the higher ranges of L concentration employed here. If the dissociated CO diffuses away in solution, no concentration dependence on L would be observed because the concentration of L is larger than that of CO and virtually all of the $Co(CO)_2NO$ intermediate would

(22) Horrocks, W. D., Jr.; Taylor, R. C. *Inorg. Chem.* **1963**, *2*, 723.
(23) Thorsteinson, E. M.; Basolo, F. *J. Am. Chem. Soc.* **1966**, *88*, 3929.
(24) Ng, D.; Zink, J. I., unpublished observations.
(25) Schramm, C.; Zink, J. I. *J. Chem. Soc.*, **1979**, *101*, 4554.
(26) Schreiner, A. F.; Brown, R. L. *J. Am. Chem. Soc.* **1968**, *90*, 3366.
(27) Feuer, H., Ed. "The Chemistry of the Nitro and Nitroso Groups", Part 1; Interscience: New York, 1969.
(28) Langford, C. H.; Gray, H. B. "Ligand Substitution Processes"; W. A. Benjamin, New York, 1965; Chapter 1.

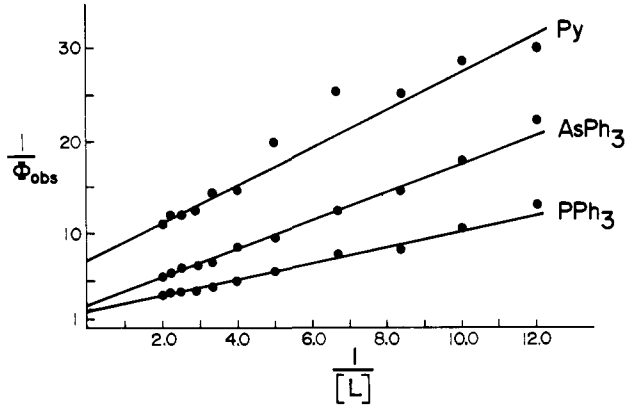

Figure 3. Plot of the reciprocal quantum yield for CO substitution vs. the reciprocal concentration of the entering ligand in cyclohexane solution.

react with L to produce $Co(CO)_2L(NO)$.

In the associative mechanism, the steady-state approximation can be applied to the excited-state intermediate. The resulting expression of most utility is

$$\frac{1}{\phi_{obsd}} = \frac{k_p + k_b}{k_p} + \left(\frac{k_p + k_b}{k_p}\right)\frac{k_1}{k_5}\frac{1}{[L]} \qquad (10)$$

In the plot of reciprocal observed quantum yield vs. reciprocal ligand L concentration, the data should fall on a straight line with an intercept $(k_p + k_b)/k_p$. Plots of the experimental quantum yields for L = PPh_3, $AsPh_3$, and pyridine are shown in Figure 3.

According to the associative interchange mechanism

$$\frac{1}{\phi_{obsd}} = \frac{k_1}{k_2[L]} + 1 \qquad (11)$$

Plots of reciprocal quantum yield vs. reciprocal ligand concentration should also be linear. However, in this case the intercepts should be 1, contrary to those observed in Figure 3.

The treatment of the dissociative mechanism is more difficult. If a standard kinetics treatment is valid, the mechanism given in eq 9 should also obey eq 11 and a reciprocal concentration vs. reciprocal quantum yield plot should be linear with an intercept of unity. On the other hand, if the Noyes scavenging theory applies,[29,30] a plot of the observed quantum yield vs. the square root of the ligand concentration should be linear. Neither of these conditions is met.

The photochemical data are most consistent with the associative mechanism for the formation of $Co(CO)_2LNO$. In contrast, both associative and a dissociative components were found in the thermal reactions.[23] The bimolecular thermal reaction was observed only for good nucleophiles such as triphenylphosphine whereas a two-term rate law was observed with triphenylarsine as the entering ligand. Thorsteinson and Basolo recognized the potential importance of the NO^- form of the nitrosyl in the bimolecular thermal reaction.[23]

The lability of the ligand L relative to that of CO in the five-coordinate intermediate is related to the numerical values of the reciprocal of the intercept of the plots in Figure 3, i.e., $k_p/(k_p + k_b)$. The experimentally determined lability order of pyridine (7.1) > $AsPh_3$ (2.4) > PPh_3 (1.5) is consistent with the π-interacting abilities of these ligands but is not correlated with their Lewis basicities. Alternatively, the ratio for labilizing L vs. CO can be interpreted by subtracting one from the intercepts, yielding k_b/k_p. In either case, the comparison is relative because k_p is not constant.

The rate constants for association of L with the bent MNO intermediate state is given by k_5/k_1, i.e., the values of the intercepts of the plots in Figure 3 divided by the corresponding slopes. The photochemically determined values for pyridine (4.1) > PPh_3 (1.6) ≥ $AsPh_3$ (1.6) follow a different order than the thermal second-order rate constants, PPh_3 >> pyridine > $AsPh_3$. The reversal of the order of pyridine and triphenylphosphine illustrates that the electronic factors in the excited-state photoreactions are different from those in the ground electronic state thermal reaction.

Metal–nitrosyl excited-state geometry changes may prove to be a general feature of the photochemistry of this group. The photochemical reactions discussed here, particularly those in the gas phase, provide strong but indirect support for such geometry changes. Many of the previously reported photoreactions of the MNO group can be interpreted in terms of excited-state MNO bending. Further studies of the MNO group are in progress to test the generality of geometry changes and their spectroscopic, photochemical, and photocatalytic consequences.

Experimental Section

Compounds. $CoNO(CO)_3$ was prepared under an atomsphere of nitrogen as described by Job and Rovang.[31] Triphenylphosphine and triphenylarsine were triply recrystallized from ethanol. Pyridine was distilled twice under nitrogen followed by three freeze–pump–thaw cycles. Aldrich Gold-Label cyclohexane was degassed and used without further purification. Triethylphosphine, purchased from Aldrich Chemical Co., was used without further purification.

Argon, nitrogen, hydrogen, methyl chloride, hydrogen chloride, *trans*-2-butene, carbon dioxide, cyanogen, and oxygen were passed through calcium chloride to remove traces of water. Nitric oxide was passed through two dry ice–acetone traps to remove traces of nitrogen dioxide. Carbon monoxide was passed through concentrated sulfuric acid followed by potassium hydroxide. Pyridine was distilled twice under nitrogen followed by three freeze–pump–thaw cycles.

Gas-Phase Studies. A cylindrical glass cell with 2-in. diameter potassium chloride windows was used for relative quantum yield determinations. The cell had a volume of approximately 100 cm^3 (4.1×10^{-3} mol of gas at 1 atm, 25 °C). A vacuum stopcock attached to a female S14/20 ground-glass joint allowed evacuation and filling. The window-cell junctions were sealed by using lightly greased O-rings. Grease was carefully excluded from the cell interior as it absorbs nitrosyltricarbonylcobalt. The cell fit into a Perkin-Elmer 521 infrared spectrophotometer and a Cary 14 UV–visible spectrophotometer for following the progress of gas-phase reactions and analyzing gaseous photoproducts. Between runs the cell was disassembled for cleaning and repolishing of windows.

Relative quantum yields were measured by using the 405- and 436-nm lines of 1000-watt high-pressure mercury–xenon lamp. The gas cell is first filled with reactant gas. Nirtosyltricarbonylcobalt, a deep red liquid possessing a high vapor pressure, was introduced into the IR cell in the liquid phase. At room temperature it evaporated within several seconds. Approximately 0.5 μL of $Co(CO)_3NO$ ($\simeq 4.2 \times 10^{-6}$ mol) was injected directly into the cell by using a 10-μL microsyringe. As the photoreaction is quite air-sensitive, this step was performed under a very strong flow of nitrogen into the outer flange of the stopcock connection. The mixture in the cell represented a reactant:cobalt mole ratio of approximately 1000:1.

In the cases of triethylphosphine and pyridine the cell was first filled with hydrogen. The reactant was then added as a liquid via microsyringe. The quantum yields for the reaction of the cobalt complex with Lewis bases were ligand concentration dependent. For assurance of accurate control of concentration, cyclohexane solutions were prepared in an inert atmosphere drybox (approximately 0.5 μL of ligand in 3 μL of solution), and these more workable liquid volumes injected into the cell. The vapor pressures of all liquids introduced are sufficiently high that all liquid evaporated. A test run of pure cyclohexane showed that it had no discernable effect on quantum yields at these concentrations. The following concentrations of ligand were used: pyridine, 3.4×10^{-6} mol ([L]/[Co] = 0.8/1.0; triethylphosphine, 8.0×10^{-6} mol [L]/[Co] = 2.0/1.0); 3.4×10^{-6} mol ([L]/[Co] = –0.8/1.0); 2.5×10^{-6} mol ([L]/[Co] = 0.6/1.0).

The disappearance of $Co(CO)_3NO$ was monitored by using the nitrosyl stretch at 1825 cm^{-1}. A working curve of intensity vs. concentration was used. As a reaction proceeded, clouds of solid precipitate formed, causing an increase in scattered light. Also, windows were partially obscured by deposits in some cases. To account for these losses in actual intensity of 405-nm light reaching the complex, the amount of light transmitted by the cell was monitored with a 1P28 photomultiplier. The photoproducts tricarbonylnitrosylcobalt, dicarbonyl(triethylphosphine)-

(29) Noyes, R. M *J. Am Chem. Soc.* **1955**, *77*, 2042.
(30) Noyes, R. M. *J. Am. Chem. Soc.* **1957**, *78*, 5486.
(31) Job, R.; Rovang, J. *Synth. React. Inorg. Met.-Org. Chem.* **1976**, *6*, 367.

nitrosylcobalt, dicarbonylnitrosylpryidylcobalt, nitric oxide, nitrous oxide, nitrogen oxide, nitrosyl chloride, and carbon monoxide were identified by their characteristic infrared bands. Nitrogen dioxide gas reacted with the potassium chloride cell windows to form potassium nitrate and nitrosyl chloride. Potassium nitrate has a sharp infrared absorption band at 1350 cm^{-1} which remained after cell evacuation. Nitrosyl chloride decomposed in the beam to yield nitric oxide and chlorine gas. Nitrosyl chloride reacts photochemically with $Co(CO)_3NO$ to produce NO_2 but no N_2O. The black powdered products from the photolysis of nitrosyltricarbonylcobalt in the presence of argon, nitrogen, and hydrogen were analyzed for cobalt content according to literature procedures.[32] In each case approximately 90 ± 10% of the material was cobalt.

Solid photoproduct from the reaction with hydrogen chloride was analyzed for cobalt[32] and chlorine[33] content according to literature procedures. Anal. Calcd for $CoCl_2$: Co, 45.4; Cl, 54.6. Found: Co, 45.3; Cl 54.4. For production of the solid photoproducts, a 500-cm^3 vessel containing about 50 μL of $Co(CO)_3NO$ was used.

The cell used for the gas phase ionic conductivity examination of the excited state was a modification of that used for relative quantum yield determinations. Electrodes consisted of 1.0 × 2.0 cm sections of copper foil aligned parallel to one another and perpendicular to the window and separated from the window by 1 mm and from one another by 1.0 cm. A set of double 2-mm slits (1.0 cm apart, the nearest being 0.5 cm from the outside edge of the cell window) assured that no light fell directly onto the cathode. The electrodes were connected to a Heathkit Model PS4 400 volt power supply and a Keithley Model 153 microvolt-ammeter in series. A bias of 400 V was applied to the electrodes during operation, resulting in a field of 400 V cm^{-1}. The system was tested by inserting a bare 50-V bulb filament between the electrodes. When the cell was evacuated and the filament heated, photoelectron current flow from filament to anode down to the 100-pA region was reproducibly registered.

Photon flux of 300-450-nm light through the slits was about 10^{15} photons s^{-1}. Absorbance by the complex at 0.5 torr over the first two centimeters of pathlength was approximately 1×10^{-2}. At a population of the MLCT state of unity efficiency, the excitation rate would be about 10^{13} molecules s^{-1}, producing a maximum current flow on the order of 10^{13} electrons s^{-1} or about 1 μA. This current is 4 orders of magnitude higher than the limit of detectability for the apparatus.

Solution-Phase Photochemistry. Cyclohexane solutions (4.00 mL) containing 6.75×10^{-3} M $Co(CO)_3NO$ and varying concentrations of entering ligand were prepared by mixing standard solutions of the cobalt complex and the ligand. From each sample solution, 2.70 mL were transferred by volumetric syringe into the irradiation cell. The remainder of the solution served as the thermal blank. All manipulations were performed in a nitrogen atmosphere drybox. All ligand concentrations were expressed in units of [L]/[Co].

Photolysis was carried out by using an optical train consisting of a Hg-Xe 1000-W high-pressure lamp and appropriate filters to isolate the 405- and 436-nm lines. The photon flux, 5×10^{-6} photons s^{-1}, was determined by using potassium ferrioxalate actinometry.[21] Sealed 1-cm Cary cells or 10 cm long Pyrex test tubes containing a ministir bar were used. The cell or tube was capped in the drybox and used throughout the entire irradiation to prevent contamination with atmospheric oxygen. Irradiated solutions and thermal blanks were transferred to infrared cells in air. Irradiation times ranged from 1 to 12 min for solutions containing entering ligands and were 90 min for solutions containing no ligand.

Starting material disappearance and product appearance were monitored by the nitrosyl infrared stretch bands on a Perkin-Elmer 421 infrared spectrophotometer using 0.1-mm sodium chloride cells. Electronic absorption spectra were measured on a Cary 15 UV-visible spectrophotometer. Absorption vs. concentration working curves were constructed to determine the extinction coefficient of the nitrosyl stretch band of $Co(CO)_3NO$. For each absorbance determination the average of six intensity measurements was used. Reproducibility of ±3% was realized by using these techniques.

Each quantum yield was determined twice and the average value reported. The rates of product appearance match those of starting material disappearance within experimental error. All photoreactions were run to 20% or less conversion.

Acknowledgment. The support of the National Science Foundation is gratefully acknowledged. The authors also thank David Ng for preliminary solution-phase photochemical studies.

(32) Young, R. S. "The Analytical Chemistry of Cobalt"; Pergamon Press: New York, 1966; p 443.
(33) Kodama, K. "Methods of Inorganic Analysis", Wiley: New York, 1963; p 443.

Imidazolate- and Oxo-Bridged Metalloporphyrins

John T. Landrum,[1] David Grimmett,[1] Kenneth J. Haller,[2] W. Robert Scheidt,[2] and Christopher A. Reed*[1]

Contribution from the Departments of Chemistry, University of Southern California, Los Angeles, California 90007, and University of Notre Dame, Notre Dame, Indiana 46556.
Received September 12, 1980

Abstract: Urea-linked tetraphenylporphyrin dimers have been synthesized with bridging imidazolate ligands between Fe(II)/Fe(II), Mn(II)/Mn(II), and Mn(II)/Co(II) centers. Magnetic susceptibility measurements down to 4 K show that imidazolate is a relatively weak mediator of antiferromagnetic coupling in these complexes ($-J$ = 2-5 cm^{-1}). The heteronuclear Mn(II)/Co(II) dimer, an $S = {}^5/_2/S = {}^1/_2$ spin model for the heme a_3/Cu_B active site of cytochrome oxidase, has $-J$ = 5 cm^{-1}. Thus, there is little support for the role of histidyl imidazolate as a bridging ligand between Fe(III) and Cu(II) in cytochrome oxidase where $-J > 200$ cm^{-1}. The magnetic, chemical, and X-ray structural properties of the μ-oxo ferric dimer of the face-to-face porphyrin have been investigated. Crystal data for $[Fe_2(C_{89}H_{56}N_{10}O)]O{\cdot}H_2O{\cdot}2$toluene follow: triclinic, a = 14.004 (6) Å, b = 22.995 (6) Å, c = 13.192 (4) Å, α = 101.45 (2)°, β = 93.91 (2)°, γ = 80.40 (2)°; space group $P\bar{1}$; Z = 2. The average Fe-N distance in the biporphyrin is 2.075 Å, and the average Fe-O distance is 1.787 Å. The iron atoms are displaced 0.60 and 0.65 Å from the mean porphinato planes. The Fe-O-Fe angle is distinctly nonlinear with a value of 161.4°; a water molecule forms a hydrogen-bonding network between the oxo ligand and the hydrogen atoms of the urea link which joins the two halves of the biporphyrin. The two porphinato planes are not coplanar, having a dihedral angle of 15.8°.

The existence of strongly interacting metal sites in bi- and tetranuclear metalloproteins such as hemocyanin, copper oxidases, hemerythrin, superoxide dismutase, and cytochrome oxidase provides an additional impetus for gaining an understanding of the coordination chemistry principles which are unique to multimetal systems.[3] Antiferromagnetic coupling mediated by imidazolate- and oxo-bridging ligands is of particular interest[4-8] as

(1) University of Southern California.
(2) University of Notre Dame.
(3) Cohen, I. A. *Struct. Bonding (Berlin)* **1980**, *40*, 1-37.

0002-7863/81/1503-2640$01.25/0